# Negatively Charged Lipids as a Potential Target for New Amphiphilic Aminoglycoside Antibiotics
## A BIOPHYSICAL STUDY*

**Guillaume Sautrey**[‡1,2], **Micheline El Khoury**[‡1], **Andreia Giro dos Santos**[‡], **Louis Zimmermann**[§], **Magali Deleu**[¶], **Laurence Lins**[¶], **Jean-Luc Décout**[§], and **Marie-Paule Mingeot-Leclercq**[‡3]

*From the [‡]Université Catholique de Louvain, Louvain Drug Research Institute, Pharmacologie Cellulaire et Moléculaire, Avenue E. Mounier 73, UCL B1.73.05 Bruxelles, Belgium, the [§]Département de Pharmacochimie Moléculaire, Université de Grenoble, Alpes/ CNRS, UMR 5063, ICMG FR 2607, 470 Rue de la Chimie, BP 53, F-38041 Grenoble, France, and the [¶]Laboratoire de Biophysique Moleculaire aux Interfaces, Université de Liège, Gembloux Agro-Bio Tech, Passage des Déportés, 2, B-5030 Gembloux, Belgium*

Bacterial membranes are highly organized, containing specific microdomains that facilitate distinct protein and lipid assemblies. Evidence suggests that cardiolipin molecules segregate into such microdomains, probably conferring a negative curvature to the inner plasma membrane during membrane fission upon cell division. 3′,6-Dinonyl neamine is an amphiphilic aminoglycoside derivative active against *Pseudomonas aeruginosa*, including strains resistant to colistin. The mechanisms involved at the molecular level were identified using lipid models (large unilamellar vesicles, giant unilamelllar vesicles, and lipid monolayers) that mimic the inner membrane of *P. aeruginosa*. The study demonstrated the interaction of 3′,6-dinonyl neamine with cardiolipin and phosphatidylglycerol, two negatively charged lipids from inner bacterial membranes. This interaction induced membrane permeabilization and depolarization. Lateral segregation of cardiolipin and membrane hemifusion would be critical for explaining the effects induced on lipid membranes by amphiphilic aminoglycoside antibiotics. The findings contribute to an improved understanding of how amphiphilic aminoglycoside antibiotics that bind to negatively charged lipids like cardiolipin could be promising antibacterial compounds.

Multidrug-resistant microbial pathogens (1, 2) have become a worldwide problem that threatens the efficacy of many drugs commonly used to treat patients suffering from severe infections. Approximately 10% of all hospital-acquired infections are the results of *Pseudomonas aeruginosa* infections, a Gram-negative, opportunistic human pathogen. This pathogen infects immunosuppressed patients, leading to high fatality rates in patients hospitalized with cancer, cystic fibrosis, and burns. To confront this challenge, it is crucial to develop new antibiotics and/or new targets.

The bacterial cell membrane shares similarities with mammalian cell membranes, including the presence of functionally differentiated regions. These distinct assemblies of proteins and/or lipids (3) are related to the regulation of many core processes, such as chromosomal and cell division-related events (4, 5). Membrane curvature is potentially responsible for preferential lipid self-assembly behaviors as well as osmosensing (6) and folding of membrane proteins (7).

Cardiolipin (CL)[4] is a lipid located primarily in the inner membrane of Gram-negative bacteria like *Pseudomonas aeruginosa* or *Escherichia coli* (8, 9). In some bacteria like *Salmonella*, this lipid has also been found in the outer membrane (10, 11). Cardiolipin has been described for its predisposition to be organized into clusters (12). This structurally unusual phospholipid carries two negative charges (13) due to its dimeric structure consisting of two phosphatidyl residues connected by a glycerol bridge and four associated fatty acyl chains, which are characterized by a high degree of symmetry and unsaturation (14). Cardiolipin is known for its sensitivity to stressors, such as the addition of organic solvents, high salt content, or quaternary ammonium compounds (15). Another striking characteristic of cardiolipin is the comparatively small cross-section of its headgroup relative to the cross-section of its four large tail groups. This discrepancy results in a molecule with a large intrinsic negative curvature (16), also described previously for phosphatidylethanolamine (PE) (17), which facilitates the insertion of membrane proteins. The cross-sectional size difference further explains the location of cardiolipin-enriched regions at the pole and/or the division septum, which can in turn relate to the polar localization of many proteins, including

[4] The abbreviations used are: CL, cardiolipin; PE, phosphatidylethanolamine; PG, phosphatidylglycerol; NPN, *N*-phenylnaphthylamine; PI, propidium iodide; POPE, 1-palmitoyl-2-oleyl-*sn*-glycero-3-phosphoethanolamine; POPG, 1-palmitoyl-2-oleyl-*sn*-glycero-3-phosphoglycerol; TF-CL, Top-Fluor®-cardiolipin; TR-PE, Texas Red®-1,2-dipalmitoyl-*sn*-glycero-3-phosphoethanolamine; MHB-CA, cation-adjusted Müller-Hinton broth; ANTS, 8-aminonaphthalene-1,3,6-trisulfonic acid; DPX, *p*-xylene-bis-pyridinium bromide; DiSC$_3$(5), 3,3′-dipropylthiadicarbocyanine iodide; LUV, large unilammelar vesicle; NAO, 10-*N*-nonyl acridine orange; GUV, giant unilamellar vesicle; R$_{18}$, octadecylrhodamine B.

those involved in cell division and osmosensing (6). In particular, in *E. coli*, cardiolipin is known to enhance the activity of the glycosyltransferase MurG involved in peptidoglycan biosynthesis (18).

A growing body of data supports the existence of segregated domains for bacterial lipids other than cardiolipin (19, 20), such as the negative curvature-inducing phosphatidylethanolamine (3, 21) and phosphatidylglycerol (PG) (21, 22), which exhibits a tendency toward a positive curvature (23).

As part of the search for new antibiotics active against Gram-negative bacteria, the cell membranes have become a promising target. We previously synthesized a series of amphiphilic neamine derivatives active against both sensitive and resistant *P. aeruginosa* (24–27). The derivatives di(2-naphthyl)propyl neamine, 3′,6-di(2-naphthyl)butyl neamine, and 3′,6-dinonyl neamine showed low toxicity and high activity, including against colistin-resistant strains (26, 27). Recently, we investigated how these amphiphilic neamine derivatives alter the bacterial outer membrane by changing the divalent metal bridges between LPSs and disordering the hydrophobic core of the LPSs (27). A bactericidal effect may arise from the specific binding of amphiphilic aminoglycosides to LPS membrane interfacial zones, inducing destabilizing lipid exchanges between the outer and the inner membranes or from their translocation to the inner membrane, possibly leading to the creation of defects/pores.

The present study sought to characterize the interaction between amphiphilic neamine derivatives and the lipids of the inner membrane of bacteria at the molecular level. We focused on the lipid cardiolipin and selected 3′,6-dinonyl neamine, one of the most promising compounds found among the 70 derivatives in our library. First, we investigated the ability of 3′,6-dinonyl neamine to induce membrane permeabilization (*N*-phenylnaphthylamine (NPN) and propidium iodide (PI) assays; calcein release) and depolarization (3,3′-dipropylthiadicarbocyanine iodide (DiSC$_3$(5)) fluorescence) of *P. aeruginosa* as well as membranes of large unilamellar vesicles (LUVs) composed from POPE/POPG/CL (60:21:11), POPE/CL (7:3), and POPE/POPG (7:3). Second, we characterized the interaction between this selected neamine derivative and the three main lipids found in bacterial membranes especially in the inner membrane of *P. aeruginosa*, PE, PG, and CL (28–31). By using 10-*N*-nonyl acridine orange (NAO) fluorescence, we compared the binding of 3′,6-dinonyl neamine to negatively charged lipids of LUVs composed of POPE/POPG/CL (60:21:11), POPE/POPG (7:3), and POPE/CL (7:3). Langmuir studies were used to determine the effect of 3′,6-dinonyl neamine on CL, POPE, and POPG monolayer organization. On giant unilamellar vesicles (GUVs) mimicking the inner membrane of *P. aeruginosa* (POPE/POPG/CL, 60:21:11), we monitored membrane permeabilization and identified the molecular mechanisms involved. In particular, by using confocal microscopy, we investigated the propensity of the amphiphilic neamine derivative to alter cardiolipin location and to induce hemifusion. The latter effect was supported by membrane fusion without content mixing, as determined by using an octadecylrhodamine B dequenching assay and 8-aminonaphthalene-1,3,6-trisulfonic acid (ANTS)/*p*-xylene-bis-pyridinium bromide (DPX) quenchinq assay, respectively) on POPE/POPG/CL, 60:21:11 LUVs. Results are discussed with respect to the changes in *P. aeruginosa* morphology observed after treatment with 3′,6-dinonyl neamine. Our findings contribute to an improved understanding of how amphiphilic aminoglycoside antibiotics acting on lipid domains, including cardiolipin clusters, could be promising antibacterial compounds.

## Experimental Procedures

Décout and colleagues (26) previously synthesized the tetratrifluoroacetate salt of 3′,6-*O*-dinonyl neamine (3′,6-dinonyl neamine), which we stored as a stock solution in water (10 mg/ml). *P. aeruginosa* strain ATCC 27853 was obtained from the Pasteur Institute (Brussels, Belgium; Prof. R. Vanhoof). POPE, POPG, heart bovine CL, and its fluorescent analogue TopFluor®-cardiolipin (TF-CL) were purchased from Avanti Polar Lipids (Alabaster, AL). PI, DiSC$_3$(5), NAO, Texas Red®-1,2-dipalmitoyl-*sn*-glycero-3-phosphoethanolamine (TR-PE), octadecylrhodamine B (R$_{18}$), ANTS, and DPX were ordered from Invitrogen (Paisley, Scotland, UK). Calcein, purchased from Sigma-Aldrich, was purified according to previous descriptions (32). Polydimethylsiloxane was kindly provided by Henri Burhin and Christian Bailly (UCL/SST/IMCN, Louvain-la-Neuve, France). All other analytical grade reagents were purchased from E. Merck AG.

*P. aeruginosa Culture*—We used TSA Petri dishes to grow *P. aeruginosa* ATCC 27853 overnight at 37 °C. One colony was suspended in cation-adjusted Müller-Hinton broth (MHB-CA) and incubated overnight at 37 °C on a rotary shaker (130 rpm). The bacterial suspension was diluted 10-fold in MHB-CA and incubated (300 rpm; 37 °C; 3 h) until it reached the end of the mid-logarithmic phase ($A_{620}$ ~0.7–0.8). Bacterial cells were isolated through centrifugation (3000 × *g*, 20 °C, 10 min), washed with HEPES buffer (5 mM, pH 7.4), centrifuged again, and resuspended in HEPES buffer to an $A_{600}$ of 0.05.

*Bright Field Microscopy of P. aeruginosa ATCC27853*—Phase-contrast microscopy was used to analyze the effect of 3′,6-dinonyl neamine on bacterial morphology. ATCC27853 was grown overnight at 37 °C. This preculture was diluted 100-fold in fresh MHB-CA and incubated at 37 °C in the presence of 3′,6-dinonyl neamine at its minimum inhibitory concentration (4 μg/ml, ~7 μM) as compared with controls. Every hour, small aliquots of these cultures were collected and observed using a Zeiss Axio Observer Z1 microscope equipped with a ×100 magnification oil immersion objective.

*LUV Preparation and Size Determination Using Dynamic Light Scattering Measurements*—LUVs composed of the three main lipids found in the inner membrane of *P. aeruginosa* (28–31) were prepared with the extrusion method from multilamellar vesicles. Phospholipids (5 mg/ml in CHCl$_3$/CH$_3$OH (2:1, v/v)) were mixed in the desired molar ratio, namely POPE/POPG/CL, 60:21:11; POPE/POPG, 7:3; and POPE/CL, 7:3. Multilamellar vesicles were prepared according to the freeze-thawing method in an aqueous buffer (10 mM Tris-HCl, pH 7.4), eventually containing calcein (73 mM) or KCl (150 mM). LUVs were then obtained with 10 successive extrusions of multilamellar vesicles through two superimposed track-etch polycarbonate membranes (pore size = 100 nm; Whatman Nucleo-

pore, Corning Costar Corp., Badhoevedorp, The Netherlands) using a 10-ml Thermobarrel® extruder (Lipex Biomembranes, Vancouver, Canada). For calcein-filled LUVs, Sephadex® gel filtration was used to remove the unencapsulated calcein with the minicolumn centrifugation technique (32, 33).

Dynamic light scattering measurements were used to control the size and polydispersity of the LUVs. The apparent average diameter of the suspended particles was monitored by using a Malvern Zetasizer Nano ZS® (Malvern Instruments, Ltd., Worcestershire, UK) equipped with a helium-neon laser and added back scattering detection at 173°. The LUV suspension (1 ml) was exposed to dynamic light scattering in a polystyrene cuvette, a size distribution obtained by accumulating three measurements consisting of 13 successive runs of 10 s. After the addition of a small aliquot of 3′,6-dinonyl neamine stock solution, dynamic light scattering measurements after 15 min of incubation were taken. All measurements were repeated at least three times. We used the Zetasizer Nano Software (supplied with the apparatus) to analyze the normalized intensity auto-correlation functions with the CONTIN algorithm. The phospholipid concentration in LUV suspensions was determined with a Bartlett phosphate assay (34); iso-osmotic buffers were used to make any necessary adjustments.

*GUV Preparation*—GUVs were prepared by the electroformation method (35). We mixed lipids in respective molar ratios of POPE/POPG/CL, 60:21:11. GUVs were labeled with TR-PE (0.1 mol%) for permeabilization studies and with TR-PE (0.1 mol%) and TF-CL (0.2 mol%) for PE and CL visualization. The lipid mixture was spread (2.5 $\mu g/cm^2$) on a glass slide coated with indium tin oxide and dried for 15 min under vacuum. To build the electroformation chamber, the first slide was covered with a second indium tin oxide-coated slide spaced with poly-dimethylsiloxane containing 5% fumed silica. The electroformation chamber was filled with buffer (2.5 mM Tris-HCl, pH 7.4, and 0.2 M sucrose), closed with polydimethylsiloxane. The GUVs were formed by applying a sinusoidal alternating current of 500 Hz and 3.25 V for 2 h at 45 °C.

The GUVs were detached from the indium tin oxide-coated slide by moving an air bubble within the electroformation chamber. The aqueous volume was completely collected. 50 $\mu l$ of GUVs were introduced into an observation cell composed of a glass slide and a coverslip spaced by a silicon spacer. Then 150 $\mu l$ of buffer (2.5 mM Tris-HCl, pH 7.4, and 0.2 M glucose), with and without the addition of 3′,6-dinonyl neamine, were added to the observation cell; the content was stirred gently and protected from light for 15 min before the observation using microscopy at room temperature. The 3′,6-dinonyl neamine concentration was adjusted for each sample to maintain a drug/lipid ratio comparable with that in the LUV experiments. The lipid concentration was determined based on a calibration curve that represents the TR-PE fluorescence intensity recorded with an LS55 spectrofluorimeter (PerkinElmer Ltd., Beaconsfield, UK) (emission at 595 nm (slit 15 nm) and excitation at 555 nm (slit 10 nm)).

*Outer and Inner Bacterial Membrane Permeabilization*—We examined the permeabilization of the outer membrane by determining the fluorescence of NPN, which is highly dependent on the polarity of the environment. When the barrier properties of the outer membrane in Gram-negative bacteria are compromised, NPN is accumulated in the hydrophobic core of the outer membrane, and the fluorescence intensity is increased (36, 37). The experiment was performed as described elsewhere (27) with some modifications; the optical density of the bacterial suspension was set to $A_{600}$ of 0.05, and the NPN concentration was set to 1 $\mu M$. Five min after the addition of 3′,6-dinonyl neamine, the NPN fluorescence spectrum was recorded (5 accumulated scans in a range of 350–550 nm, slits 2.5 nm, 500 nm/min) at an excitation wavelength of 350 nm (LS55 spectrofluorimeter, PerkinElmer Ltd.). The data were normalized based on the fluorescence of NPN in the presence of colistin 10 $\mu M$ (100%).

The permeabilization of the inner bacterial membrane was determined with a membrane-impermeable fluorescent dye (PI), which is accessible to permeabilized bacteria only. A stock solution of PI (3 mM in pure water) was diluted $10^3$-fold with the bacterial suspension ($A_{600}$ of 0.05). 3′,6-Dinonyl neamine in HEPES buffer, at final concentrations ranging from 1 to 10 $\mu M$, was added to the PI-containing bacterial suspension in 96-well microplates. The fluorescence intensity was measured with a SpectraMax® M3 microplate reader at 25 °C after 15 min of stabilization (Molecular Devices, Sunnyvale, CA) for excitation and emission wavelengths of 540 and 610 nm, respectively. The data were normalized based on the fluorescence intensity measured in the presence of either 150 $\mu M$ quaternary ammonium hexadecyltrimethylammonium bromide (positive control, 100%) (38) or imipenem (negative control, 0%).

*Bacterial Membrane Depolarization*—We investigated the depolarization of bacterial membranes and LUVs by using the membrane potential-sensitive fluorescent probe $DiSC_3(5)$. Once $DiSC_3(5)$ is localized predominantly in a polarized membrane, its $\lambda_{max}$ is close to 678 nm. After membrane depolarization, $DiSC_3(5)$ is released into the aqueous medium, increasing the fluorescence intensity (39).

*P. aeruginosa* ATCC 27853 were grown and isolated as described above. Before the addition of $DiSC_3(5)$, the bacterial suspension ($A_{600} = 0.05$) was supplemented with EDTA (50 mM in HEPES buffer) and with KCl (2.5 M in HEPES buffer) to 0.2 and 100 mM, respectively. The $DiSC_3(5)$ probe was added (0.4 $\mu M$ final concentration), and the bacterial suspension was incubated in the dark for 30 min at 37 °C. 3′,6-Dinonyl neamine was distributed in a 96-well microplate; thereafter, the bacterial suspension containing $DiSC_3(5)$ was added to obtain a final derivative concentration ranging from 0.5 to 10 $\mu M$. A preliminary experiment, without bacterial cells, was performed to ensure that the presence of 3′,6-dinonyl neamine had no effect on $DiSC_3(5)$ fluorescence. To determine the ability of 3′,6-dinonyl neamine to depolarize the bacterial membrane, the membrane was artificially hyperpolarized before adding the amphiphilic aminoglycoside derivative using KCl and EDTA to allow the passage of $DiSC_3(5)$ across the outer membrane. An increase in $DiSC_3(5)$ fluorescence indicates an equilibrium of the extra- and intracellular $K^+$ content. The $K^+$-specific ionophore valinomycin was used as a positive control (40). Readings were performed with excitation and emission wavelengths of 622 and 670 nm, respectively.

*Permeabilization of LUVs and GUVs*—The permeabilizing effect of 3′,6-dinonyl neamine was investigated by using calcein-filled LUVs and GUVs. Calcein-filled LUVs composed of POPE/POPG/CL (60:21:11), POPE/POPG (7:3), and POPE/CL (7:3) were prepared using 10 mM Tris-HCl (pH 7.4) and calcein 73 mM (390 mosmol/liter measured with the freezing point technique (Knauer osmometer automatic, Berlin, Germany)); the LUVs were diluted with 10 mM Tris-HCl (pH 7.4) buffer containing 159 mM NaCl. A small amount of 3′,6-dinonyl neamine was added to 1 ml of calcein-filled LUVs to obtain concentrations ranging from 0.1 to 5 $\mu$M. The release of calcein from the LUVs and its dilution in the medium resulted in fluorescence dequenching (41), which was monitored over time. Experiments were performed at 25 °C using an LS55 spectrofluorimeter (PerkinElmer) with excitation and emission wavelengths fixed at 472 and 512 nm, respectively. For each experiment, the percentage of calcein that was released was determined by measuring the initial fluorescence and the maximum fluorescence obtained after the addition of Triton X-100 (0.05%). Control experiments were performed with conventional aminoglycosides (gentamicin and neomycin B), neamine (showing no significant calcein release), and colistin, all at 10 $\mu$M.

Calcein-filled GUVs labeled with TR-PE were electroformed (as described above) using a Tris-HCl (2.5 mM, pH 7.4, 0.2 M sucrose) buffer supplemented with calcein (20 $\mu$M). The GUVs were diluted 10-fold in buffer (2.5 mM Tris-HCl, pH 7.4, 0.2 M glucose) containing a 3′,6-dinonyl neamine/anionic lipid ratio comparable with that used in calcein-filled LUV experiments. After incubation in the dark, samples were observed through confocal microscopy. Calcein was observed in the green channel. About 20 snapshots of single and joined GUVs were collected, and the difference of fluorescence of calcein between inside and outside was measured using AxioVision® software.

*LUV Depolarization*—Dissipation of membrane potential using LUVs was determined according to Tiriveedhi and Butko (42). Briefly, LUVs composed of POPE/POPG/CL (60:21:11), POPE/POPG (7:3), and POPE/CL (7:3) were prepared in 10 mM Tris-HCl (pH 7.4), 150 mM KCl buffer and diluted at 5 $\mu$M in 10 mM Tris-HCl (pH 7.4), 150 mM NaCl in the presence of 4 $\mu$M DiSC$_3$(5). 10 $\mu$M valinomycin was added immediately to the cuvette, and the value of the membrane potential was adjusted according to the Nernst equation,

$$\Delta \Psi = \frac{RT}{ZF} \ln \left( \frac{C_{in}}{C_{out}} \right) \quad \text{(Eq. 1)}$$

where $\Delta\psi$ is the membrane potential, $R$ is the universal gas constant, $T$ is the absolute temperature, $Z$ is the charge of the transported ion, $F$ is the Faraday constant, and $C$ is the concentration of potassium ions. The DiSC$_3$(5) emission at 668 nm (slit 15 nm) was recorded after an excitation wavelength of 615 nm (slit 10 nm) using an LS55 spectrofluorimeter (PerkinElmer). After stabilization of the fluorescence signal, 3′,6-dinonyl neamine was added successively with increasing concentrations ranging from 0.25 to 3 $\mu$M.

*Binding to Anionic Lipid*—NAO has been widely used to visualize CL and PG domains in bacterial membranes through spe-

cific Stokes shift of the emission peak when bound to anionic lipids (43, 44). The ability of 3′,6-dinonyl neamine to displace NAO from its binding to anionic lipids in LUVs was measured by following the increase of NAO fluorescence. The self-quenching of the emission peak at 520 nm was titrated by NAO to determine the optimal NAO concentration. Fluorescence measurements were recorded 5 min after the successive addition of NAO (3 mM in ethanol) to 1 ml of LUV suspension (5 $\mu$M phosphate). The optimal NAO concentration for LUVs composed of POPE/POPG/CL (60:21:11), POPE/POPG (7:3), and POPE/CL (7:3) was 2.1, 1.5, and 2.3 $\mu$M, respectively. These values are close to the theoretical concentration corresponding to the ratios NAO/POPG (1:1) and NAO/CL (2:1).

In a 96-well microplate, 3′,6-dinonyl neamine was added to NAO-containing LUVs in triplicate. Fluorescence intensities were measured following a 15-min stabilization period at room temperature. The NAO fluorescence was recorded at 25 °C using a SpectraMax® M3 Microplate Reader (Molecular Devices, Sunnyvale, CA) with excitation and emission wavelengths of 488 and 520 nm, respectively. The data were normalized based on the fluorescence intensity in LUV-free wells (maximum fluorescence of NAO in solution, 100%) and 3′,6-dinonyl neamine-free wells (minimum fluorescence of lipid-bound NAO, 0%).

*Confocal Microscopy of GUVs*—GUVs were widely used to investigate physicochemical properties of lipid mixtures, including the formation of lipid domains linked to phase separation processes and vesicle fusion (45). The GUVs were observed in the red channel for TR-PE (excitation at 561 nm and emission at 617 nm) and in the green channel for TF-CL (excitation at 488 nm and emission at 530 nm). An Axio Observer Z1 inverted microscope (Carl Zeiss, Jena, Germany) equipped with a model CSU-X1 spinning disk (Yokogawa Electric Corp., Tokyo, Japan) and a Plan-Apochromat ×100/1.40 numerical aperture oil DIC M27 objective (Carl Zeiss) was used. Images were recorded and analyzed with an Axio-CamMR3 camera using Carl Zeiss AxioVision® version 4.8.2 software.

*Membrane Fusion and Content Mixing of LUVs*—Fusion of membranes and content mixing were monitored on LUVs. First, R$_{18}$, a lipid-soluble probe, was incorporated into a lipid membrane as its fluorescence became self-quenched in direct proportion with its concentration (in a 1–9-mol % range). A decrease in its surface density (46) is associated with an increase in the fluorescence intensity of the preparation. Labeled liposomes were obtained by incorporating R$_{18}$ in the dry lipid film at a molar ratio of 5.7% with respect to the total lipids and diluted to a concentration of 5 $\mu$M in average lipid. They were then mixed with unlabeled liposomes adjusted to the same concentration, at a ratio of 1:4. The variation of the fluorescence intensity of the preparation was thereafter followed at room temperature during 5 min, using a $\lambda_{ex}$ of 560 nm and a $\lambda_{em}$ of 590 nm. Second, an ANTS-DPX assay was used for monitoring content mixing. Lipid films were emulsified in buffer A (10 mM Tris-HCl, 150 mM NaCl) containing 25 mM ANTS and/or 90 mM DPX and thereafter extruded. The unincorporated ANTS and DPX were removed on a Sephadex G-50 column equilibrated with buffer A (47). ANTS liposomes (1:3, v/v) were

added to DPX liposomes (2:3, v/v), and fluorescence of ANTS was followed at 530 nm (excitation at 384 nm). Mixing of ANTS and DPX is registered as a decrease in ANTS fluorescence due to quenching by DPX. Leakage was measured with liposomes containing both ANTS and DPX. Calcium chloride at 25 mM was used as a positive control.

*Surface Pressure-Area Compression Isotherms*—To examine the effect of 3′,6-dinonyl neamine on lipid packing, surface pressure-area compression isotherms were recorded with an automated Langmuir trough (Microtrough X, Kibron, Helsinki, Finland) equipped with a rectangular Teflon trough (width = 5.8 cm, length = 23.1 cm), two hydrophilic Delrin mobile barriers (symmetric compression), a platinum Wilhelmy wire, and a temperature probe. The system was enclosed in a plexiglass box, and the temperature was maintained at 24.8 ± 0.7 °C.

The cleanliness of the surface was ensured by aspiration of the subphase surface before each experiment. The platinum wire was cleaned by rinsing with isopropyl alcohol and heating to a red glow between two experiments. A buffer (10 mM Tris-HCl, pH 7.4) was used as the subphase. Either POPE, POPG, or CL (initially dissolved at a concentration of 0.5 mg/ml in $CHCl_3$/MeOH (2:1, v/v)) was spread on the surface drop by drop with a microsyringe (Hamilton). After an equilibration time of 15 min, the film was compressed at a rate of 5 mm/min. 3′,6-Dinonyl neamine was solubilized in the subphase at 0.1 $\mu$M before spreading the lipid. Each compression isotherm was repeated at least two times; the relative S.D. in surface pressure and area was ≤5%.

## Results

*Morphology of P. aeruginosa*—The effect of 3′,6-dinonyl neamine on *P. aeruginosa* morphology was assessed through bright field microscopy. *P. aeruginosa* was treated (Fig. 1*A*, *right*) with the 3′,6-dinonyl neamine derivative at a concentration equal to its minimum inhibitory concentration for 7 h. The control (Fig. 1*A*, *left*) was grown under the same conditions but in the absence of 3′,6-dinonyl neamine.

Initially, both treated and untreated samples showed the classical rod-shaped morphology of *Pseudomonas*. The shape was maintained after 7 h in the control conditions. In contrast, in the presence of 3′,6-dinonyl neamine, shape and length were altered. Moreover, microcolonies were observed in the control conditions, whereas no division was observed even after 7 h of incubation in the presence of 3′,6-dinonyl neamine. Because cell division largely involves membranes, this effect on *P. aeruginosa* morphology prompted us to investigate the ability of 3′,6-dinonyl neamine to modify the biophysical properties of bacterial membranes.

*P. aeruginosa Outer and Inner Membrane Permeabilization*—To investigate whether changes in morphology induce changes in membrane permeability that could be involved in antibacterial effect, we used specific probes (NPN and PI) to monitor outer and inner membrane permeation, respectively. A permeabilized outer membrane accumulates NPN into its hydrophobic core accompanied by an increase in fluorescence (36–38). Likewise, when PI passes through the cell membrane and binds to nucleic acids, fluorescence intensity increases (48).
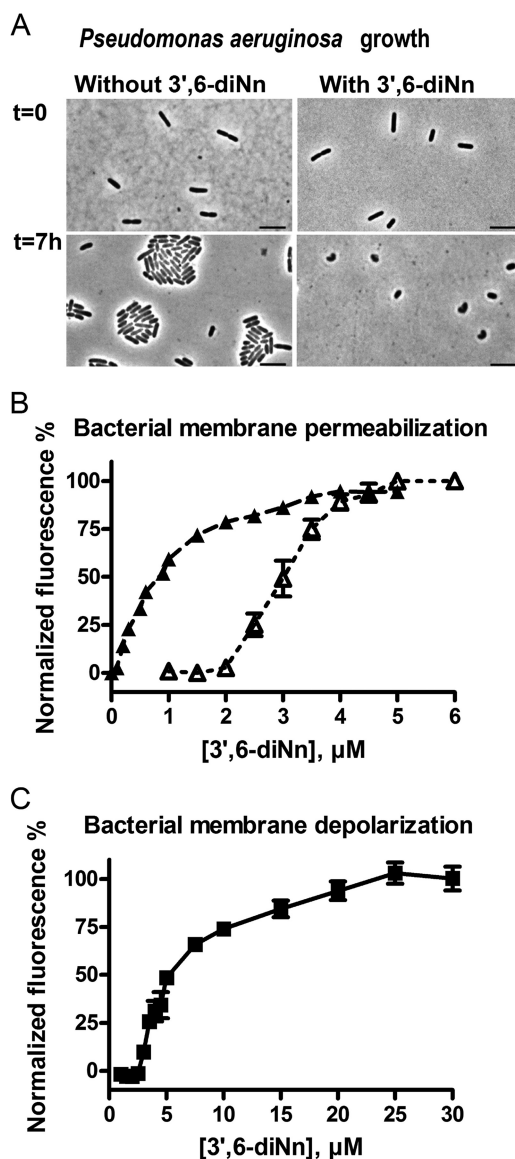


FIGURE 1. *A*, phase-contrast images of *P. aeruginosa* ATCC 27853 non-treated (*left*) and treated (*right*) with 3′,6-dinonyl neamine at its minimum inhibitory concentration for 7 h at 37 °C. *Black scale bar*, 4 $\mu$m. *B*, outer (▲) and inner (△) membrane permeabilization of *P. aeruginosa* induced by 3′,6-dinonyl neamine as assessed by enhancing NPN and PI fluorescence, respectively. *C*, membrane depolarization of *P. aeruginosa* induced by 3′,6-dinonyl neamine and assessed through changes in $DiSC_3$(5) fluorescence intensity; valinomycin and imipen were used as positive and negative controls, respectively. *B* and *C*, n = 3; *error bars*, S.E.

Fig. 1*B* shows that 3′,6-dinonyl neamine induced a dose-dependent permeabilization of both the outer and inner membranes. The effect on the outer membrane was observed immediately after the addition of the amphiphilic neamine derivative, whereas 2 $\mu$M was required to induce inner membrane permeabilization. A plateau value was reached at around 4 $\mu$M for both outer and inner membrane permeabilization. Consequently, 3′,6-dinonyl neamine concentration required to alter membrane permeability was slightly higher for the inner than for the outer membrane.

*P. aeruginosa Membrane Depolarization*—We further examined the ability of 3′,6-dinonyl neamine to depolarize the inner bacterial membrane (Fig. 1*C*). The membrane potential-sensi-

tive probe DiSC$_3$(5), known to accumulate in hyperpolarized cell membranes, where its fluorescence is quenched, was used (40). When depolarization occurs, the probe is released in solution, resulting in fluorescence intensity increase (39). Depolarization was observed from around 3.5 μM 3′,6-dinonyl neamine. A plateau value was reached at 25 μM (Fig. 1C).

*LUV Membrane Permeabilization and Depolarization*—To gain further insight into the ability of 3′,6-dinonyl neamine to permeabilize membranes, we monitored the release of calcein (32, 41) from LUVs composed of POPE/POPG/CL (60:21:11), POPE/CL (7:3), and POPE/POPG (7:3). Regardless of lipid composition (Fig. 2A), we observed a dose-dependent calcein release from LUVs incubated with 3′,6-dinonyl neamine at concentrations ranging from 0.25 to 1.7 μM. After the addition of 3′,6-dinonyl neamine at 1 μM, >80% of calcein was released in the presence of cardiolipin, whereas only around 50% was released when cardiolipin was absent. These differences could reflect differences in mechanism (all-or-none *versus* graded mechanisms) (49), but further studies are required to confirm this.

Fig. 2B shows the effect of 3′,6-dinonyl neamine on DiSC$_3$(5) fluorescence for liposomes. The cumulative addition of 3′,6-dinonyl neamine showed an increase in DiSC$_3$(5) fluorescence, reflecting its release from the depolarized membrane. For the three lipid compositions selected, depolarization was observed from 0.5 μM. The rate of the process was higher for liposomes containing cardiolipin.

All together, these results showed the critical role of cardiolipin for membrane permeabilization and depolarization induced by 3′,6-dinonyl neamine. In the presence of PG, a very different pattern was obtained for both processes.

*NAO Staining of LUVs*—To identify the roles of CL and PG in 3′,6-dinonyl neamine-induced membrane depolarization, we used NAO, a fluorescent cationic amphiphilic probe known to bind to negatively charged lipids and used in cell imaging, to reveal PG- or CL-containing lipid domains (43, 44).

LUVs (POPE/POPG/CL, 60:21:11; POPE/POPG, 7:3; and POPE/CL, 7:3) were labeled with NAO, and increasing concentrations of 3′,6-dinonyl neamine were added. An increase in NAO fluorescence, depending on the 3′,6-dinonyl neamine concentration, was observed, indicating that NAO was displaced from LUVs as a result of 3′,6-dinonyl neamine binding to negatively charged lipids (Fig. 2C). In the presence of cardiolipin, EC$_{50}$ values were higher as compared with EC$_{50}$ values for liposomes without cardiolipin, reflecting a preferential binding of 3′,6-dinonyl neamine to cardiolipin.

*GUV Permeabilization and Cardiolipin Location*—To directly visualize the effects of 3′,6-dinonyl neamine on membrane permeabilization, the comparatively large size of GUVs was exploited by using microscopy (Fig. 3, *left*) (50). When GUVs were incubated with concentrations of 3′,6-dinonyl neamine selected to maintain a drug/lipid ratio comparable with that for LUV experiments, a striking first observation was the presence of two types of populations: single and joined liposomes. A similar behavior has also been reported for antimicrobial peptides (51). Hemifused liposomes represented ~60% of the total population. Based on the green fluorescence of calcein, we quanti-
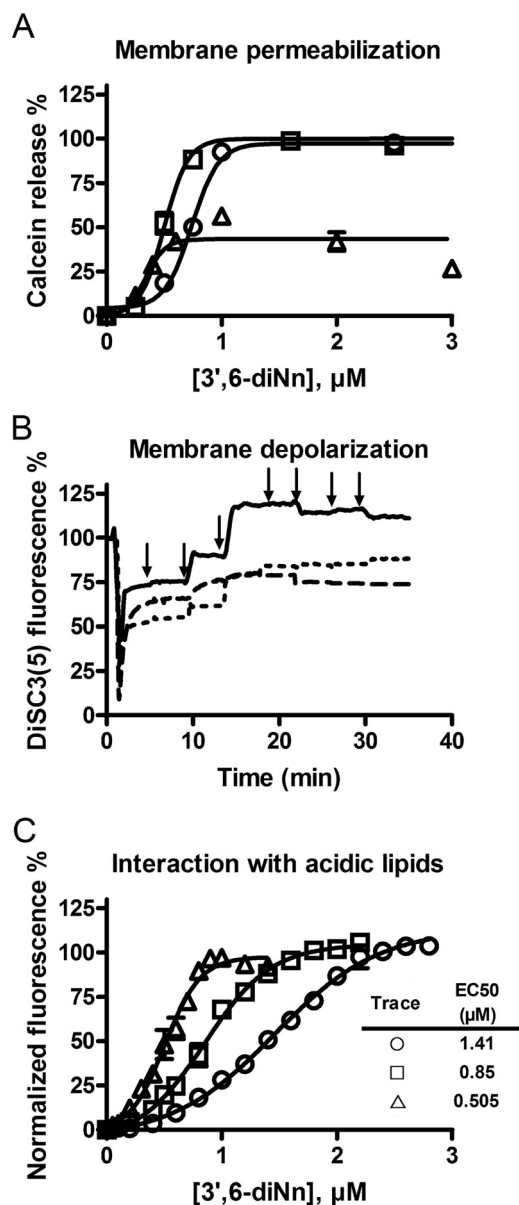


FIGURE 2. *A*, dose-dependent calcein leakage from LUVs consisting of POPE/POPG/CL (60:21:11) (□), POPE/POPG (7:3) (△), and POPE/CL (7:3) (○). Values were normalized after 10 min of incubation with 3′,6-dinonyl neamine. No significant calcein release was observed with gentamicin, neomycin B, and neamine, whereas rapid calcein release was induced by colistin (data not shown). *B*, dose-dependent membrane depolarization induced by 3′,6-dinonyl neamine and assessed through changes in DiSC$_3$(5) fluorescence on LUVs composed of POPE/POPG/CL (60:21:11) (*solid line*), POPE/POPG (7:3) (*dashed line*), and POPE/CL (7:3) (*dotted line*). Valinomycin was added at $t = 0$ min, and 3′,6-dinonyl neamine was added consecutively in increasing concentrations of 0.25, 0.5, 1, 1.5, 2, 2.5, and 3 μM. *Arrows*, time of addition of 3′,6-dinonyl neamine. Mean S.E. values of all data points of POPE/POPG/CL, POPE/POPG, and POPE/CL depolarization curves were 1.456 ± 0.1267, 3.555 ± 0.05015, and 5.332 ± 0.1949, respectively. Valinomycin and imipenem were used as positive and negative controls, respectively. *C*, binding of 3′,6-dinonyl neamine to anionic lipids in LUVs of POPE/POPG/CL (60:21:11) (□), POPE/POPG (7:3) (△), and POPE/CL (7:3) (○) assessed by displacing of the NAO dye from LUVs and monitored through fluorescence increase. Fluorescence intensities were normalized (see "Experimental Procedures"), and data were analyzed through a nonlinear regression according to the Boltzmann sigmoid equation characterized by EC$_{50}$ values. *A–C*, $n = 3$; *error bars*, S.E.

fied the membrane permeabilization induced by the 3′,6-dinonyl neamine derivative by calculating the difference in calcein fluorescence intensity between inside and outside, in com-
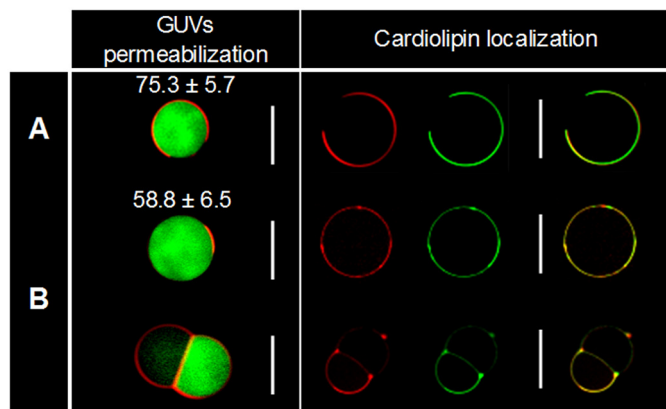
FIGURE 3. **Membrane permeabilization (*left*) and cardiolipin localization (*right*) of POPE/POPG/CL (60:21:11) GUVs: control (*A*) and non-hemi-fused and hemifused liposomes treated for 1 h with 3',6-dinonyl neamine (*B*) monitored through confocal microscopy.** Calcein release (*green*) entrapped in TR-PE-labeled GUVs (*red*) composed of POPE/POPG/CL (60:21:11) was monitored (*left*). Note the average green fluorescent intensity (arbitrary units) and S.D. ($p < 0.05$ according to Student's *t* test, indicating a difference in fluorescence intensities between the control and treated conditions). Shown on the *right* is a visualization of PE and CL localization in POPE/POPG/CL control GUVs (*A*) and GUVs treated with 3',6-dinonyl neamine (*B*) using the red TR-PE and the green TF-CL fluorescent dyes, (*n* = 3). *White scale bars*, 10 μm.

parison with control samples. For single liposomes, we observed a statistically significant release of calcein from GUVs. For joined liposomes, membrane permeabilization was not uniform throughout the joined structures. After initial changes, no more changes occurred during the 1–6-h incubation period.

Because GUVs also allow us to visualize the formation of lipid domains linked to phase separation processes (50), we determined the effect of 3',6-dinonyl neamine on cardiolipin localization. Fig. 3 (right) shows that after incubation with 3',6-dinonyl neamine, CL was co-localized with PE in small clusters, sections with increased membrane curvature, and fusion points in the joined GUV population. Moreover, a clear overall lipid reorganization was observed.

*Size, Membrane Fusion, and Content Mixing of LUVs*—To further characterize the effect of 3',6-dinonyl neamine in changes in vesicle morphology resulting in hemifused liposomes, we first monitored the size of LUVs (POPE/POPG/CL, 60:21:11) incubated with 3',6-dinonyl neamine (Fig. 4*A*). The results showed a progressive increase of the apparent radius, which did not exceed 400 nm. The effect started at concentrations close to 0.5 μM and reached a plateau value at 2 μM 3',6-dinonyl neamine.

Second, hemifusion suggested by confocal microscopy on GUVs implies the fusion of the outer layers of each vesicle where the stable bilayer at the interface of the independent compartments is composed of the two inner layers (52). To confirm this process, we monitored membrane fusion and content mixing by using the self-quenching properties of R$_{18}$ and the quenching of ANTS by DPX (46, 47), respectively. The addition of 3',6-dinonyl neamine to POPE/POPG/CL (60:21:11) LUVs showed a rapid membrane fusion (Fig. 4*B*) without content mixing (Fig. 4*C*). Once membrane fusion was induced, the fusion rate was independent of the concentration of the derivative (Fig. 4*B*). Results obtained on GUVs independently labeled with two fluorescent probes confirmed lipid
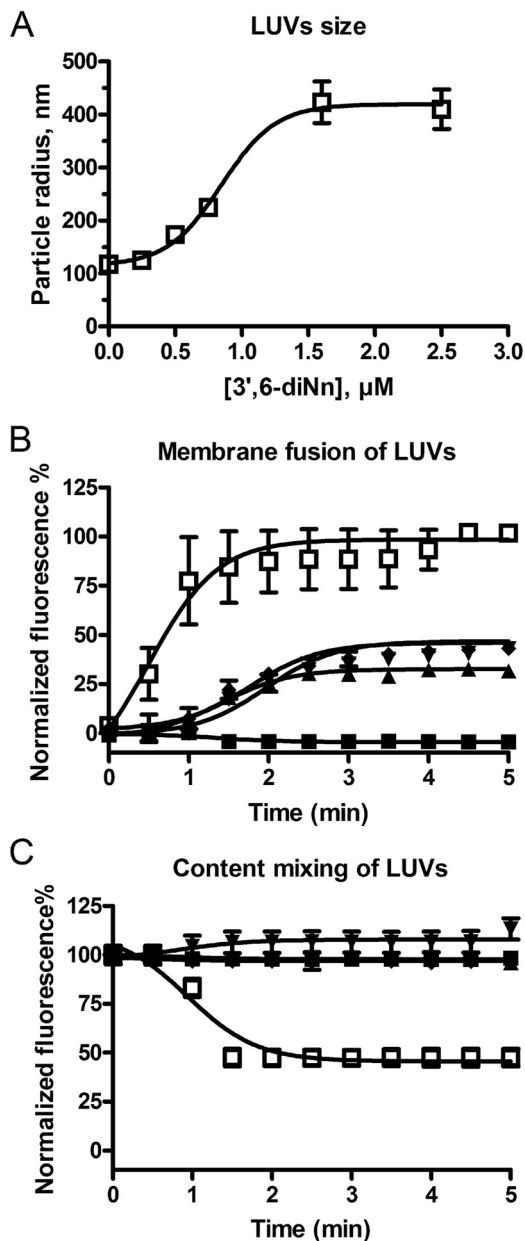


FIGURE 4. *A*, dose-dependent effect of 3',6-dinonyl neamine on the size of LUVs composed of POPE/POPG/CL (60:21:11) (□). *B*, membrane fusion of LUVs (POPE/POPG/CL, 60:21:11) as assessed by R$_{18}$ fluorescence dequenching; *C*, content mixing of LUVs studied by ANTS/DPX fluorescence quenching assays on POPE/POPG/CL (60:21:11) liposomes incubated in the presence of 3',6-dinonyl neamine at concentrations of 0.1 (■), 0.50 (▲), 0.75 (▼), and 1.0 μM (♦). Triton X-100 at 0.1% (□) and calcium chloride at 25 mM (□) were used as positive control for lipid and aqueous fusion, respectively. No significant effect was observed with neamine (data not shown). In *A–C*, *n* = 3; *error bars*, S.E.

mixtures (data not shown). Taken together, these results suggest the presence of a stable single bilayer obtained concomitantly with the fusion of the outer layer of fusing GUVs as present in hemifusion intermediates.

*Mean Molecular Area*—To obtain insight into the effect of 3',6-dinonyl neamine on individual lipids and especially on the mean molecular area, we determined the compression isotherms corresponding to the lipid monolayers spread on a subphase containing 3',6-dinonyl neamine. The isotherms were shifted to higher molecular areas than the pure buffer subphase,
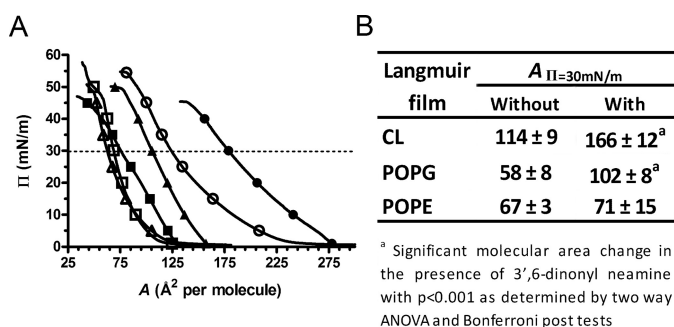
| Langmuir film | $A_{\Pi=30mN/m}$ | |
|---|---|---|
| | Without | With |
| CL | 114 ± 9 | 166 ± 12[a] |
| POPG | 58 ± 8 | 102 ± 8[a] |
| POPE | 67 ± 3 | 71 ± 15 |

[a] Significant molecular area change in the presence of 3′,6-dinonyl neamine with p<0.001 as determined by two way ANOVA and Bonferroni post tests

FIGURE 5. **Interactions of 3′,6-dinonyl neamine with pure phospholipid monolayers spread on a Tris-HCl buffer (10 mM, pH 7.4) at 25 °C.** *A*, surface pressure (Π)-molecular area compression isotherms of POPE (□ and ■), POPG (△ and ▲), and CL (○ and ●) in the absence (*open symbols*) and in the presence (*solid symbols*) of 3′,6-dinonyl neamine 0.1 μM. The *dotted line* represents a surface pressure of Π = 30 millinewtons/m. Each compression isotherm is representative of at least three independent experiments. *B*, comparison of the molecular areas at Π = 30 millinewtons/m of each phospholipid monolayer in the absence and in the presence of 0.1 μM 3′,6-dinonyl neamine (*n* = 3).

although to a much lower extent for POPE compared with POPG and CL (Fig. 5). At 30 millinewtons/m, a value close to the estimated surface pressure of biological membranes *in vivo* (31–34 millinewtons/m (53, 54), the mean molecular area for POPE was not significantly modified by the presence of 3′,6-dinonyl neamine in the subphase (67 ± 3 *versus* 71 ± 15); however, for POPG and CL, the mean molecular area increased by ~1.8 and 1.6, respectively (Fig. 5). This discrepancy indicates a much higher adsorption of 3′,6-dinonyl neamine into POPG or CL than into POPE. The shift of the mean molecular area was not significantly different between POPG and CL.

## Discussion

Amphiphilic neamine derivatives showed high antibacterial activity, including against susceptible and resistant *Pseudomonas aeruginosa*, and a low toxicity as measured on macrophages (26). The molecular shape of these antibacterials and the flexibility of the hydrophobic moiety of the 3′,6-dialkyl neamine derivatives are critical characteristics for their interactions with LPS of *P. aeruginosa* and their effect on outer membrane permeabilization (27). One unanswered critical question to further decipher the molecular mechanism of action of these promising antibacterials is to know whether they are able to interact with lipids found in the inner membrane of Gram-negative bacteria.

Selecting one of the most promising identified derivatives (26), 3′,6-dinonyl neamine, we characterized (i) the interaction of this compound with cardiolipin and phosphatidylglycerol, the two main negatively charged lipids of the inner membrane of *P. aeruginosa*; (ii) the lipid reorganization and clustering of cardiolipin; (iii) the joining of vesicles probably due to hemifusion process; and (iv) the membrane permeabilization and depolarization favored by the presence of cardiolipin.

The lipid phase and the molecular shape of the lipids could be of crucial importance for these effects. Even fatty acid chain identity is highly variable; cardiolipin is characterized by a high degree of chain unsaturation (14, 55–57) and a global negative spontaneous curvature (58–60). In turn, cardiolipin leads to highly bent structures and domains in disordered phases. Based

on our results, the ability of the amphiphilic neamine derivative to bind to lipids exhibiting a high negative curvature (such as cardiolipin) could be responsible for lipid membrane reorganization. By affecting curvature stress in the bilayer, a modulation of the lateral phase distribution of cardiolipin induced by 3′,6-dialkyl neamine could in turn lead to hemifusion.

According to this hypothesis, the amphiphilic aminoglycoside claims space in the headgroup layer of cardiolipin domains and in that of other cone-shaped lipid species that provide more bulk in the hydrophobic acyl chain layer than in the headgroup layer. Therefore, the lipid curvature-driven force hypothesis could be a potential candidate for explaining the permeabilizing effect induced by amphiphilic neamine derivatives. The cone shape of these compounds could fit with the characteristic inverted cone shape of cardiolipin. Such an effect could contribute to promote the subsequent increase in the area of one monolayer with respect to the other (61). Membrane reorganization and lipid segregation could result ultimately in membrane permeabilization and membrane reorganization with hemifusion and/or stalk intermediates (62–64).

Previous studies have shown that divalent cations trigger the hemifusion process by interacting with negatively charged lipids. The proposed mechanism involves reduced repulsion and a dehydration of lipid headgroups (65, 66) and an increase of membrane tension (67) in the outer leaflet (68). The hemifusion intermediate could directly lead to the formation of a pore, or it might expand radially into a hemifusion diaphragm with the distal membrane leaflets remaining separated and a bilayer formed by the inner monolayers for both vesicles (62).

Our results show that, similar to what is observed for divalent cations, 3′,6-dinonyl neamine (i) interacts specifically with negatively charged lipids and leads to (ii) clustering of negatively curved lipids CL and PE and (iii) an increase in their mean molecular area. Furthermore, the present work shows the fusion of the outer leaflet lipids and the absence of content mixing, indicating an unrestricted hemifusion process (*i.e.* a non-productive fusion pore opening after onset of lipid mixing) (69).

Based on our results, we hypothesize that clustering of negatively curved lipids like CL induced changes in localized curvature leading to membrane protrusions and fusion of the outer leaflet into hemifusion intermediates, which would be followed by its expansion into the hemifusion diaphragm formed by the two formerly inner membrane leaflets.

This hypothesis is in agreement with the tendency of CL and PE to undergo a lamellar-to-hexagonal phase transition occurring via a mechanism involving stalk formation (70–72).

As demonstrated in this work, cardiolipin is important for LUV permeabilization and depolarization induced by 3′,6-dinonyl neamine. This might also be related to the ability of 3′,6-dinonyl neamine to cause morphological changes in *P. aeruginosa* with loss of its typical rod shape into more spherical bacteria. Cardiolipin is preferentially localized at both the pole and division sites of rod-shaped bacterial cells (73, 74). Such cardiolipin-enriched domains may be explained by the extensive network of hydrogen bonds with the other important negatively charged lipids (phosphatidylglycerol) (3). This lipid segregation as well as the ability to disrupt van der Waals packing

(75) might be related to critical changes in bacterial physiology. As an example, perturbations of cardiolipin domains in *E. coli* might be responsible for the changes in the activity of MurG (18), a glycosyltransferase involved in the cytoplasmic stage of peptidoglycan synthesis (76). Impairment in the ability of MurG to form a complex with proteins involved in lateral envelope growth and cell division (77) could explain both the decreased length of *P. aeruginosa* and the transition from rod-shaped to spherical bacteria induced by amphiphilic aminoglycoside antibiotics. The existence of cardiolipin domains could further explain why the effect is specific to bacterial over mammalian membranes. In fact, bacterial membranes (i) are more negatively charged than eukaryotic membranes; (ii) contain a higher proportion of negative intrinsic curvature lipids, where proteins involved in the formation of the division plane are located (78, 79); and (iii) exhibit a dilational elasticity modulus that is much lower than the one found in mammalian membranes (80).

These combined observations emphasize the importance of the hydrophobic and electrostatic interactions between amphiphilic aminoglycosides and bacterial inner membrane lipids and underline the role of lipid packing. Similar to α-synuclein (81) and 2-hydroxylated fatty acid derivatives (82), amphiphilic aminoglycosides showed a high affinity for negatively charged lipids. The data permit the extension of a previous hypothesis suggesting a self-promoted uptake of conventional aminoglycosides within the bacteria (83). The hydrophobic tail added to the aminoglycoside backbone allows enhanced membrane targeting, LPS destabilization, and inner membrane penetration to reach negatively charged lipids, such as cardiolipin and phosphatidylglycerol. Interactions of the 3′,6-dinonyl neamine derivative with these lipids induced membrane permeabilization and depolarization as well as their local redistribution, which in turn resulted in decreased bacterial cell viability. These results suggest that lipid domains (such as cardiolipin platforms) displaying distinctive biophysical properties in bacterial membranes could be targeted in the development of new antibiotics.

## References

1. Fauci, A. S., and Marston, H. D. (2014) The perpetual challenge of antimicrobial resistance. *JAMA* **311,** 1853–1854
2. Payne, D. J. (2008) Desperately seeking new antibiotics. *Science* **321,** 1644–1645
3. Matsumoto, K., Kusaka, J., Nishibori, A., and Hara, H. (2006) Lipid domains in bacterial membranes. *Mol. Microbiol.* **61,** 1110–1117
4. Saxena, R., Fingland, N., Patil, D., Sharma, A. K., and Crooke, E. (2013) Crosstalk between DnaA protein, the initiator of *Escherichia coli* chromosomal replication, and acidic phospholipids present in bacterial membranes. *Int. J. Mol. Sci.* **14,** 8517–8537
5. Goehring, N. W., and Beckwith, J. (2005) Diverse paths to midcell: assembly of the bacterial cell division machinery. *Curr. Biol.* **15,** R514–R526
6. Sadeghi, S., Müller, M., and Vink, R. L. (2014) Raft formation in lipid bilayers coupled to curvature. *Biophys J.* **107,** 1591–1600
7. Gessmann, D., Chung, Y. H., Danoff, E. J., Plummer, A. M., Sandlin, C. W., Zaccai, N. R., and Fleming, K. G. (2014) Outer membrane β-barrel protein folding is physically controlled by periplasmic lipid head groups and BamA. *Proc. Natl. Acad. Sci. U.S.A.* **111,** 5878–5883
8. Kaneko, H., Takami, H., Inoue, A., and Horikoshi, K. (2000) Effects of hydrostatic pressure and temperature on growth and lipid composition of the inner membrane of barotolerant *Pseudomonas* sp. BT1 isolated from the deep-sea. *Biosci. Biotechnol. Biochem.* **64,** 72–79
9. Broniatowski, M., Mastalerz, P., and Flasiński, M. (2015) Studies of the interactions of ursane-type bioactive terpenes with the model of *Escherichia coli* inner membrane-Langmuir monolayer approach. *Biochim. Biophys. Acta* **1848,** 469–476
10. Dalebroux, Z. D., Matamouros, S., Whittington, D., Bishop, R. E., and Miller, S. I. (2014) PhoPQ regulates acidic glycerophospholipid content of the *Salmonella typhimurium* outer membrane. *Proc. Natl. Acad. Sci. U.S.A.* **111,** 1963–1968
11. Dalebroux, Z. D., Edrozo, M. B., Pfuetzner, R. A., Ressl, S., Kulasekara, B. R., Blanc, M. P., and Miller, S. I. (2015) Delivery of cardiolipins to the *Salmonella* outer membrane is necessary for survival within host tissues and virulence. *Cell Host Microbe* **17,** 441–451
12. Epand, R. M., and Epand, R. F. (2009) Lipid domains in bacterial membranes and the action of antimicrobial agents. *Biochim. Biophys. Acta* **1788,** 289–294
13. Olofsson, G., and Sparr, E. (2013) Ionization constants p$K_a$ of cardiolipin. *PLoS One* **8,** e73040
14. Schlame, M. (2008) Cardiolipin synthesis for the assembly of bacterial and mitochondrial membranes. *J. Lipid Res.* **49,** 1607–1620
15. Boeris, P. S., Domenech, C. E., and Lucchesi, G. I. (2007) Modification of phospholipid composition in *Pseudomonas putida* A ATCC 12633 induced by contact with tetradecyltrimethylammonium. *J. Appl. Microbiol.* **103,** 1048–1054
16. Dowhan, W. (1997) Molecular basis for membrane phospholipid diversity: why are there so many lipids? *Annu. Rev. Biochem.* **66,** 199–232
17. Rogasevskaia, T. P., and Coorssen, J. R. (2011) A new approach to the molecular analysis of docking, priming, and regulated membrane fusion. *J. Chem. Biol.* **4,** 117–136
18. van den Brink-van der Laan, E., Boots, J. W., Spelbrink, R. E., Kool, G. M., Breukink, E., Killian, J. A., and de Kruijff, B. (2003) Membrane interaction of the glycosyltransferase MurG: a special role for cardiolipin. *J. Bacteriol.* **185,** 3773–3779
19. Fishov, I., and Norris, V. (2012) Membrane heterogeneity created by transertion is a global regulator in bacteria. *Curr. Opin. Microbiol.* **15,** 724–730
20. Epand, R. M., and Epand, R. F. (2011) Bacterial membrane lipids in the action of antimicrobial agents. *J. Pept. Sci.* **17,** 298–305
21. Vanounou, S., Parola, A. H., and Fishov, I. (2003) Phosphatidylethanolamine and phosphatidylglycerol are segregated into different domains in bacterial membrane: a study with pyrene-labelled phospholipids. *Mol. Microbiol.* **49,** 1067–1079
22. Oliver, P. M., Crooks, J. A., Leidl, M., Yoon, E. J., Saghatelian, A., and Weibel, D. B. (2014) Localization of anionic phospholipids in *Escherichia coli* cells. *J. Bacteriol.* **196,** 3386–3398
23. Salay, L. C., Ferreira, M., Oliveira ON Jr., Nakaie, C. R., and Schreier, S. (2012) Headgroup specificity for the interaction of the antimicrobial peptide tritrpticin with phospholipid Langmuir monolayers. *Colloids Surf. B Biointerfaces* **100,** 95–102
24. Baussanne, I., Bussière, A., Halder, S., Ganem-Elbaz, C., Ouberai, M., Riou, M., Paris, J. M., Ennifar, E., Mingeot-Leclercq, M. P., and Décout, J. L.

(2010) Synthesis and antimicrobial evaluation of amphiphilic neamine derivatives. *J. Med. Chem.* **53,** 119–127

25. Ouberai, M., El Garch, F., Bussiere, A., Riou, M., Alsteens, D., Lins, L., Baussanne, I., Dufrêne, Y. F., Brasseur, R., Decout, J. L., and Mingeot-Leclercq, M. P. (2011) The *Pseudomonas aeruginosa* membranes: a target for a new amphiphilic aminoglycoside derivative? *Biochim. Biophys. Acta* **1808,** 1716–1727

26. Zimmermann, L., Bussière, A., Ouberai, M., Baussanne, I., Jolivalt, C., Mingeot-Leclercq, M. P., and Décout, J. L. (2013) Tuning the antibacterial activity of amphiphilic neamine derivatives, comparison to paromamine homologues. *J. Med. Chem.* **56,** 7691–7705

27. Sautrey, G., Zimmermann, L., Deleu, M., Delbar, A., Souza Machado, L., Jeannot, K., Van Bambeke, F., Buyck, J. M., Decout, J. L., and Mingeot-Leclercq, M. P. (2014) New amphiphilic neamine derivatives active against resistant *Pseudomonas aeruginosa* and their interactions with lipopolysaccharides. *Antimicrob. Agents Chemother.* **58,** 4420–4430

28. Lopes, S. C., Neves, C. S., Eaton, P., and Gameiro, P. (2012) Improved model systems for bacterial membranes from differing species: the importance of varying composition in PE/PG/cardiolipin ternary mixtures. *Mol. Membr. Biol.* **29,** 207–217

29. Cheng, J. T., Hale, J. D., Elliott, M., Hancock, R. E., and Straus, S. K. (2011) The importance of bacterial membrane composition in the structure and function of aurein 2.2 and selected variants. *Biochim. Biophys. Acta* **1808,** 622–633

30. Murzyn, K., Róg, T., and Pasenkiewicz-Gierula, M. (2005) Phosphatidylethanolamine-phosphatidylglycerol bilayer as a model of the inner bacterial membrane. *Biophys. J.* **88,** 1091–1103

31. Epand, R. M., Rotem, S., Mor, A., Berno, B., and Epand, R. F. (2008) Bacterial membranes as predictors of antimicrobial potency. *J. Am. Chem. Soc.* **130,** 14346–14352

32. Van Bambeke, F., Mingeot-Leclercq, M. P., Schanck, A., Brasseur, R., and Tulkens, P. M. (1993) Alterations in membrane permeability induced by aminoglycoside antibiotics: studies on liposomes and cultured cells. *Eur. J. Pharmacol.* **247,** 155–168

33. Lelkes, P. I. (1984) *Liposome Technology*, pp. 225–246, CRC Press, Inc., Boca Raton, FL

34. Bartlett, G. R. (1959) Phosphorus assay in column chromatography. *J. Biol. Chem.* **234,** 466–468

35. Angelova, M. I., Soléau, S., Méléard, P., Faucon, J. F., and Bothorel, P. (1992) Preparation of giant vesicles by external AC electric fields: kinetics and applications. In *Trends in Colloid and Interface Science VI* (Helm, C., Lösche, M., and Möhvald, H., eds) pp. 127–131, Steinkopff, Dresden, Germany

36. Loh, B., Grant, C., and Hancock, R. E. (1984) Use of the fluorescent probe 1-*N*-Phenylnaphthylamine to study the interactions of aminoglycoside antibiotics with the outer membrane of Pseudomonas aeruginosa. *Antimicrob. Agents Chemother.* **26,** 546–551

37. Wu, M., and Hancock, R. E. (1999) Interaction of the cyclic antimicrobial cationic peptide bactenecin with the outer and cytoplasmic membrane. *J. Biol. Chem.* **274,** 29–35

38. Di Pasquale, E., Salmi-Smail, C., Brunel, J. M., Sanchez, P., Fantini, J., and Maresca, M. (2010) Biophysical studies of the interaction of squalamine and other cationic amphiphilic molecules with bacterial and eukaryotic membranes: importance of the distribution coefficient in membrane selectivity. *Chem. Phys. Lipids* **163,** 131–140

39. Krasne, S. (1980) Interactions of voltage-sensing dyes with membranes. II. Spectrophotometric and electrical correlates of cyanine-dye adsorption to membranes. *Biophys. J.* **30,** 441–462

40. Smith, J. C. (1990) Potential-sensitive molecular probes in membranes of bioenergetic relevance. *Biochim. Biophys. Acta* **1016,** 1–28

41. Weinstein, J. N., Yoshikami, S., Henkart, P., Blumenthal, R., and Hagins, W. A. (1977) Liposome-cell interaction: transfer and intracellular release of a trapped fluorescent marker. *Science* **195,** 489–492

42. Tiriveedhi, V., and Butko, P. (2007) A fluorescence spectroscopy study on the interactions of the TAT-PTD peptide with model lipid membranes. *Biochemistry* **46,** 3888–3895

43. Lobasso, S., Saponetti, M. S., Polidoro, F., Lopalco, P., Urbanija, J., Kralj-Iglic, V., and Corcelli, A. (2009) Archaebacterial lipid membranes as models to study the interaction of 10-*N*-nonyl acridine orange with phospholipids. *Chem. Phys. Lipids* **157,** 12–20

44. Mileykovskaya, E., Ryan, A. C., Mo, X., Lin, C. C., Khalaf, K. I., Dowhan, W., and Garrett, T. A. (2009) Phosphatidic acid and *N*-acylphosphatidylethanolamine form membrane domains in *Escherichia coli* mutant lacking cardiolipin and phosphatidylglycerol. *J. Biol. Chem.* **284,** 2990–3000

45. Alam, J. M., Kobayashi, T., and Yamazaki, M. (2012) The single-giant unilamellar vesicle method reveals lysenin-induced pore formation in lipid membranes containing sphingomyelin. *Biochemistry* **51,** 5160–5172

46. Hoekstra, D., de Boer, T., Klappe, K., and Wilschut, J. (1984) Fluorescence method for measuring the kinetics of fusion between biological membranes. *Biochemistry* **23,** 5675–5681

47. Düzgüneş, N., Faneca, H., and Lima, M. C. (2010) Methods to monitor liposome fusion, permeability, and interaction with cells. *Methods Mol. Biol.* **606,** 209–232

48. Niven, G. W., and Mulholland, F. (1998) Cell membrane integrity and lysis in *Lactococcus lactis*: the detection of a population of permeable cells in post-logarithmic phase cultures. *J. Appl. Microbiol.* **84,** 90–96

49. Apellániz, B., Nieva, J. L., Schwille, P., and García-Sáez, A. J. (2010) All-or-none versus graded: single-vesicle analysis reveals lipid composition effects on membrane permeabilization. *Biophys. J.* **99,** 3619–3628

50. Wesołowska, O., Michalak, K., Maniewska, J., and Hendrich, A. B. (2009) Giant unilamellar vesicles: a perfect tool to visualize phase separation and lipid rafts in model systems. *Acta Biochim. Pol.* **56,** 33–39

51. Wadhwani, P., Epand, R. F., Heidenreich, N., Bürck, J., Ulrich, A. S., and Epand, R. M. (2012) Membrane-active peptides and the clustering of anionic lipids. *Biophys. J.* **103,** 265–274

52. Meers, P., Ali, S., Erukulla, R., and Janoff, A. S. (2000) Novel inner monolayer fusion assays reveal differential monolayer mixing associated with cation-dependent membrane fusion. *Biochim. Biophys. Acta* **1467,** 227–243

53. Demel, R. A., Geurts van Kessel, W. S., Zwaal, R. F., Roelofsen, B., and van Deenen, L. L. (1975) Relation between various phospholipase actions on human red cell membranes and the interfacial phospholipid pressure in monolayers. *Biochim. Biophys. Acta* **406,** 97–107

54. Marsh, D. (1996) Lateral pressure in membranes. *Biochim. Biophys. Acta* **1286,** 183–223

55. Ghorbal, S. K., Chatti, A., Sethom, M. M., Maalej, L., Mihoub, M., Kefacha, S., Feki, M., Landoulsi, A., and Hassen, A. (2013) Changes in membrane fatty acid composition of *Pseudomonas aeruginosa* in response to UV-C radiations. *Curr. Microbiol.* **67,** 112–117

56. Bernal, P., Segura, A., and Ramos, J. L. (2007) Compensatory role of the *cis-trans*-isomerase and cardiolipin synthase in the membrane fluidity of *Pseudomonas putida* DOT-T1E. *Environ. Microbiol.* **9,** 1658–1664

57. Minkler, P. E., and Hoppel, C. L. (2010) Separation and characterization of cardiolipin molecular species by reverse-phase ion pair high-performance liquid chromatography-mass spectrometry. *J. Lipid Res.* **51,** 856–865

58. Kozlovsky, Y., Chernomordik, L. V., and Kozlov, M. M. (2002) Lipid intermediates in membrane fusion: formation, structure, and decay of hemifusion diaphragm. *Biophys. J.* **83,** 2634–2651

59. Epand, R. F., Martinou, J. C., Fornallaz-Mulhauser, M., Hughes, D. W., and Epand, R. M. (2002) The apoptotic protein tBid promotes leakage by altering membrane curvature. *J. Biol. Chem.* **277,** 32632–32639

60. Beales, P. A., Bergstrom, C. L., Geerts, N., Groves, J. T., and Vanderlick, T. K. (2011) Single vesicle observations of the cardiolipin-cytochrome *c* interaction: induction of membrane morphology changes. *Langmuir* **27,** 6107–6115

61. Basañez, G. (2002) Membrane fusion: the process and its energy suppliers. *Cell Mol. Life Sci.* **59,** 1478–1490

62. Nikolaus, J., Warner, J. M., O'Shaughnessy, B., and Herrmann, A. (2011) The pathway to membrane fusion through hemifusion. *Curr. Top. Membr.* **68,** 1–32

63. Chernomordik, L. V., and Kozlov, M. M. (2008) Mechanics of membrane fusion. *Nat. Struct. Mol. Biol.* **15,** 675–683

64. Katsov, K., Müller, M., and Schick, M. (2004) Field theoretic study of bilayer membrane fusion. I. Hemifusion mechanism. *Biophys. J.* **87,** 3277–3290

65. Feigenson, G. W. (1986) On the nature of calcium ion binding between

phosphatidylserine lamellae. *Biochemistry* **25,** 5819–5825

66. Mattai, J., Hauser, H., Demel, R. A., and Shipley, G. G. (1989) Interactions of metal ions with phosphatidylserine bilayer membranes: effect of hydrocarbon chain unsaturation. *Biochemistry* **28,** 2322–2330

67. Ohki, S. (1982) A mechanism of divalent ion-induced phosphatidylserine membrane fusion. *Biochim. Biophys. Acta* **689,** 1–11

68. Chanturiya, A., Scaria, P., Woodle, M.C. (2000) The role of membrane lateral tension in calcium-induced membrane fusion. *J. Membr. Biol.* **176,** 67–75

69. Chernomordik, L. V., Frolov, V. A., Leikina, E., Bronk, P., and Zimmerberg, J. (1998) The pathway of membrane fusion catalyzed by influenza hemagglutinin: restriction of lipids, hemifusion, and lipidic fusion pore formation. *J. Cell Biol.* **140,** 1369–1382

70. Siegel, D. P. (1999) The modified stalk mechanism of lamellar/inverted phase transitions and its implications for membrane fusion. *Biophys. J.* **76,** 291–313

71. Ortiz, A., Killian, J. A., Verkleij, A. J., and Wilschut, J. (1999) Membrane fusion and the lamellar-to-inverted-hexagonal phase transition in cardiolipin vesicle systems induced by divalent cations. *Biophys. J.* **77,** 2003–2014

72. Siegel, D. P., and Epand, R. M. (1997) The mechanism of lamellar-to-inverted hexagonal phase transitions in phosphatidylethanolamine: implications for membrane fusion mechanisms. *Biophys J.* **73,** 3089–3111

73. Mileykovskaya, E., and Dowhan, W. (2009) Cardiolipin membrane domains in prokaryotes and eukaryotes. *Biochim. Biophys. Acta* **1788,** 2084–2091

74. Renner, L. D., and Weibel, D. B. (2011) Cardiolipin microdomains localize to negatively curved regions of *Escherichia coli* membranes. *Proc. Natl. Acad. Sci. U.S.A.* **108,** 6264–6269

75. Wydro, P. (2013) The influence of cardiolipin on phosphatidylglycerol/phosphatidylethanolamine monolayers–studies on ternary films imitating bacterial membranes. *Colloids Surf. B Biointerfaces* **106,** 217–223

76. Favini-Stabile, S., Contreras-Martel, C., Thielens, N., and Dessen, A. (2013) MreB and MurG as scaffolds for the cytoplasmic steps of peptidoglycan biosynthesis. *Environ. Microbiol.* **15,** 3218–3228

77. Mohammadi, T., Karczmarek, A., Crouvoisier, M., Bouhss, A., Mengin-Lecreulx, D., and den Blaauwen, T. (2007) The essential peptidoglycan glycosyltransferase MurG forms a complex with proteins involved in lateral envelope growth as well as with proteins involved in cell division in *Escherichia coli. Mol. Microbiol.* **65,** 1106–1121

78. Bramkamp, M., and van Baarle, S. (2009) Division site selection in rod-shaped bacteria. *Curr. Opin. Microbiol.* **12,** 683–688

79. Renner, L. D., and Weibel, D. B. (2012) MinD and MinE interact with anionic phospholipids and regulate division plane formation in *Escherichia coli. J. Biol. Chem.* **287,** 38835–38844

80. Evans, E. A., and Waugh, R. (1977) Osmotic correction to elastic area compressibility measurements on red cell membrane. *Biophys. J.* **20,** 307–313

81. Stöckl, M., Fischer, P., Wanker, E., and Herrmann, A. (2008) α-Synuclein selectively binds to anionic phospholipids embedded in liquid-disordered domains. *J. Mol. Biol.* **375,** 1394–1404

82. Ibarguren, M., López, D. J., Encinar, J. A., González-Ros, J. M., Busquets, X., and Escribá, P. V. (2013) Partitioning of liquid-ordered/liquid-disordered membrane microdomains induced by the fluidifying effect of 2-hydroxylated fatty acid derivatives. *Biochim. Biophys. Acta* **1828,** 2553–2563

83. Chopra, I. (1988) Molecular mechanisms involved in the transport of antibiotics into bacteria. *Parasitology* **96,** S25–S44

**Negatively Charged Lipids as a Potential Target for New Amphiphilic Aminoglycoside Antibiotics: A BIOPHYSICAL STUDY**

Guillaume Sautrey, Micheline El Khoury, Andreia Giro dos Santos, Louis Zimmermann, Magali Deleu, Laurence Lins, Jean-Luc Décout and Marie-Paule Mingeot-Leclercq

Access the most updated version of this article at doi: 10.1074/jbc.M115.665364

Alerts:
- When this article is cited
- When a correction for this article is posted

Click here to choose from all of JBC's e-mail alerts

This article cites 81 references, 17 of which can be accessed free at
http://www.jbc.org/content/291/26/13864.full.html#ref-list-1